

A 9% efficiency of flexible Mo-foil-based $Cu_2ZnSn(S, Se)_4$ solar cells by improving CdS buffer layer and heterojunction interface

Quan-Zhen Sun(孙全震), Hong-Jie Jia(贾宏杰), Shu-Ying Cheng(程树英), Hui Deng(邓辉), Qiong Yan(严琼), Bi-Wen Duan(段碧雯), Cai-Xia Zhang(张彩霞), Qiao Zheng(郑巧), Zhi-Yuan Yang(杨志远), Yan-Hong Luo(罗艳红), Qing-Bo Men(孟庆波), and Shu-Juan Huang(黄淑娟)

Citation: Chin. Phys. B, 2020, 29 (**12**): 128801. DOI: 10.1088/1674-1056/abb7fe
Journal homepage: http://cpb.iphy.ac.cn; http://iopscience.iop.org/cpb

What follows is a list of articles you may be interested in

A 9% efficiency of flexible Mo-foil-based $Cu_2ZnSn(S, Se)_4$ solar cells by improving CdS buffer layer and heterojunction interface

Quan-Zhen Sun(孙全震), Hong-Jie Jia(贾宏杰), Shu-Ying Cheng(程树英), Hui Deng(邓辉), Qiong Yan(严琼), Bi-Wen Duan(段碧雯), Cai-Xia Zhang(张彩霞), Qiao Zheng(郑巧), Zhi-Yuan Yang(杨志远), Yan-Hong Luo(罗艳红), Qing-Bo Men(孟庆波), and Shu-Juan Huang(黄淑娟)
Chin. Phys. B, 2020, 29 (**12**): 128801. DOI: 10.1088/1674-1056/abb7fe

Highly efficient bifacial semitransparent perovskite solar cells based on molecular doping of CuSCN hole transport layer

Shixin Hou(侯世欣), Biao Shi(石标), Pengyang Wang(王鹏阳), Yucheng Li(李玉成), Jie Zhang(张杰), Peirun Chen(陈沛润), Bingbing Chen(陈兵兵), Fuhua Hou(侯福华), Qian Huang(黄茜), Yi Ding(丁毅), Yuelong Li(李跃龙), Dekun Zhang(张德坤), Shengzhi Xu(许盛之), Ying Zhao(赵颖), Xiaodan Zhang(张晓丹)
Chin. Phys. B, 2020, 29 (**7**): 078801. DOI: 10.1088/1674-1056/ab99ae

Current improvement in substrate structured Sb_2S_3 solar cells with $MoSe_2$ interlayer

Lu Liu(刘璐), Sheng-Li Zhang(张生利), Jian-Yu Wu(吴建宇), Wei-Huang Wang(王伟煌), Wei Liu(刘玮), Li Wu(武莉), Yi Zhang(张毅)
Chin. Phys. B, 2020, 29 (**5**): 058801. DOI: 10.1088/1674-1056/ab8220

Two-step processed efficient perovskite solar cells via improving perovskite/PTAA interface using solvent engineering in PbI_2 precursor

Cao-Yu Long(龙操玉), Ning Wang(王宁), Ke-Qing Huang(黄可卿), Heng-Yue Li(李恒月), Biao Liu(刘标), Jun-Liang Yang(阳军亮)
Chin. Phys. B, 2020, 29 (**4**): 048801. DOI: 10.1088/1674-1056/ab7744

Improvement in IBC-silicon solar cell performance by insertion of highly doped crystalline layer at heterojunction interfaces

Hadi Bashiri, Mohammad Azim Karami, Shahramm Mohammadnejad
Chin. Phys. B, 2017, 26 (**10**): 108801. DOI: 10.1088/1674-1056/26/10/108801

A 9% efficiency of flexible Mo-foil-based $Cu_2ZnSn(S, Se)_4$ solar cells by improving CdS buffer layer and heterojunction interface*

Quan-Zhen Sun(孙全震)[1,†], Hong-Jie Jia(贾宏杰)[1,†], Shu-Ying Cheng(程树英)[1,2,‡], Hui Deng(邓辉)[1,§], Qiong Yan(严琼)[1,3], Bi-Wen Duan(段碧雯)[4], Cai-Xia Zhang(张彩霞)[1,2], Qiao Zheng(郑巧)[1,2], Zhi-Yuan Yang(杨志远)[1], Yan-Hong Luo(罗艳红)[4], Qing-Bo Men(孟庆波)[4], and Shu-Juan Huang(黄淑娟)[5]

[1] *College of Physics and Information Engineering, Institute of Micro-Nano Devices and Solar Cells, Fuzhou University, Fuzhou* 350108, *China*
[2] *Jiangsu Collaborative Innovation Center of Photovoltaic Science and Engineering, Changzhou* 213164, *China*
[3] *Key Laboratory of Green Perovskites Application of Fujian Province Universities, Fujian Jiangxia University, Fuzhou* 350108, *China*
[4] *Beijing National Laboratory for Condensed Matter Physics, Institute of Physics, Chinese Academy of Sciences, Beijing* 100190, *China*
[5] *Australian Centre for Advanced Photovoltaics, School of Photovoltaic and Renewable Energy Engineering, University of New South Wales, Sydney* 2052, *Australia*

(Received 11 May 2020; revised manuscript received 28 August 2020; accepted manuscript online 14 September 2020)

Flexible $Cu_2ZnSn(S,Se)_4$ (CZTSSe) solar cells show great potential applications due to low-cost, nontoxicity, and stability. The device performances under an especial open circuit voltage (V_{OC}) are limited by the defect recombination of CZTSSe/CdS heterojunction interface. We improve the deposition technique to obtain compact CdS layers without any pinholes for flexible CZTSSe solar cells on Mo foils. The efficiency of the device is improved from 5.7% to 6.86% by highquality junction interface. Furthermore, aiming at the S loss of CdS film, the S source concentration in deposition process is investigated to passivate the defects and improve the CdS film quality. The flexible Mo-foil-based CZTSSe solar cells are obtained to possess a 9.05% efficiency with a V_{OC} of 0.44 V at an optimized S source concentration of 0.68 mol/L. Systematic physical measurements indicate that the S source control can effectively suppress the interface recombination and reduce the V_{OC} deficit. For the CZTSSe device bending characteristics, the device efficiency is almost constant after 1000 bends, manifesting that the CZTSSe device has an excellent mechanical flexibility. The effective improvement strategy of CdS deposition is expected to provide a new perspective for promoting the conversion efficiency of CZTSSe solar cells.

Keywords: flexible solar cells, CdS deposition, heterojunction interface, defect passivation

PACS: 88.40.hj, 88.40.jn, 81.10.Dn **DOI:** 10.1088/1674-1056/abb7fe

1. Introduction

The $Cu_2ZnSn(S,Se)_4$ (CZTSSe) is expected to be one of the most promising absorber materials for thin-film solar cells due to its tunable band gap and earth-abundant elemental constituents.[1–5] According to the substrate, there are two different CZTSSe solar cells, *i.e.* flexible and rigid solar cells. The flexible CZTSSe solar cells have attracted much attention due to their great advantages in the photovoltaic industry such as building-integrated photovoltaic and unmanned aircraft systems.[6] Recently, the highest power conversion efficiency (PCE) of flexible CZTSSe solar cells reached 10.34%.[7] However, there is still a great gap between actual PCE and the Schockley–Queisser (SQ) limit efficieny (33%),[8] in an especial open circuit voltage (V_{OC}).[9,10] The main bottlenecks, limiting V_{OC} and PCE of CZTSSe thin film solar cells, are the defect recombinations in absorber and heterojunction interfaces.[11]

The CdS buffer layer with a high carrier concentration and fantastic n-type properties leads to its wide applications in solar cells.[12] Highquality CdS buffer layer is a key point for high performance of CZTSSe solar cells by passivating CZTSSe/CdS heterojunction interface defects and improving the junction quality.[11] Wei *et al.* improved the quality of the interface by depositing two CdS layers for CZTSSe solar cells and obtained a 10.19% efficiency.[13] Zhang *et al.* passivated the CZTSSe/CdS heterojunction interface defects by using UV-ozone treatment to improve PCE from 3.18% to 5.55%.[14] Sun *et al.* used the ultra-thin SnO_2 intermediate in the CZTS/CdS interface to passivate defects and improve V_{OC} and *FF* of the device.[15] Therefore, improving CdS layer quality and passivating CZTSSe/CdS interface defects are effective ways to overcome the bottlenecks of device performance.

For flexible devices, the CZTSSe/CdS heterojunction

*Project supported by the National Natural Science Foundation of China (Grant Nos. 62074037, 61574038, 51961165108, and 51972332), the Natural Science Foundation of Fujian Province, China (Grant No. 2017J01503), the Education and Scientific Research Project of Fujian Province, China (Grant No. JAT190010), the Open Project Program of the State Key Laboratory of Photocatalysis on Energy and Environment, China (Grant No. SKLPEE-202011), and Fuzhou University, China.

†These authors contributed equally to this work.
‡Corresponding author. E-mail: sycheng@fzu.edu.cn
§Corresponding author. E-mail: denghui@fzu.edu.cn

© 2020 Chinese Physical Society and IOP Publishing Ltd

would bear stronger stress at bending state. Hence the interface defects are more detrimental to the performance of flexible device, which cause greater V_{OC} deficits. The CdS layer deposited on a flexible substrate has more unstable factors than on a rigid substrate, such as the deformation in the deposition process. That would result in poor CdS quality and more interface defects. Therefore, the optimization of CdS layer for flexible device is significant to reduce interface defects and improve the performance. The CdS buffer layer is usually fabricated by chemical bath deposition (CBD) method. In our previous work,[16] the $CdSO_4$ and thiourea powders were directly added to reaction process. And the flexible CZTSSe solar cell obtained a 6.78% efficiency with a low V_{OC}. There may arise a problem that the uneven concentration of thiourea in the liquid might lead a poorquality CdS film to form. The CBD process,[17–19] where the reactants are in the form of solution added, would effectively avoid the above problem. The poor quality and S loss in CdS film result in deep level defects, showing a large influence on the heterojunction interface and device performance.[20] Therefore, the technical investigation and defect passivation of CdS layer are emphasised to reduce interface combination and improve PCE.

In this work, we focus on the quality of CdS film and CZTSSe/CdS heterojunction interface of flexible Mo-foil-based solar cells. Two CdS deposition methods (P-CBD and S-CBD) are investigated to obtain the dense CdS layers without pinholes and improve the V_{OC} and PCE. Subsequently, the quality of CdS layer is further optimized by controlling the content of S source in CBD process to overcome S loss in CdS film and passivate defects. Systematic characterizations manifest that the device with the optimized buffer layer and S source control can obviously passivate interface defects and reduce carrier recombination. The PCE of flexible Mo-foil-based CZTSSe solar cells is significantly improved to 9.05%.

2. Experiment

2.1. CdS film deposition

The CdS layer was prepared by chemical bath deposition (CBD). The common CBD method of CdS film is to add $CdSO_4$ and thiourea powders to reaction process, which is named P-CBD method. Specifically, the 0.0768-g $CdSO_4$ powder ($CdSO_4{\cdot}8/3H_2O$, Aladdin, 99.99%) and 250-mL deionized water were mixed together in a beaker at 70 °C. Then 20-mL ammonium hydroxide (NH_4OH, AR 25%–28%) was added into the mixture and stirred for 10 min. The CZTSSe films were soaked in the solution, and then 0.11-g thiourea (CH_4N_2S, AR $\geq$ 99.0%) powder was added into the above reaction solution for 12 min–16 min to obtain the CdS film. This work updated the CBD method by simultaneously adding $CdSO_4$ and thiourea solution for depositing CdS film, named S-CBD method. A 20-mL $CdSO_4$ aqueous solution with 0.02-mol/L, 20-mL ammonium hydroxide and 205-mL deionized water were mixed together in a beaker. After being stirred for 5 min at 70 °C, a 25-mL thiourea aqueous solution with 0.068 mol/L was added into the solution. The samples were placed in the above solution for 12 min–16 min to obtain the CdS film. In addition, we prepared thiourea aqueous solutions with three different concentrations, *i.e.*, 0.340 mol/L (5 times 0.068 mol/L), 0.680 mol/L (10 times 0.068 mol/L), 1.020 mol/L (15 times 0.068 mol/L). The CdS film prepared by the P-CBD method was named P-CBD-1; these CdS films prepared by the S-CBD method were called P-CBD-x, with $x = 1$, 5, 10, 15 times thiourea concentration (0.068 mol/L) for the conventional S-CBD, respectively.

2.2. Fabrication of solar cells

The CZTSSe solar cells were fabricated on electropolished Mo foils with the device structure being Mo foil/CZTSSe/CdS/i-ZnO/ITO/Ag. The Mo foil was polished at a voltage of 2.5 V and room temperature for 1.5 min in the methanol solution of sulfuric acid (H_2SO_4:CH_3OH=7:1) to obtain the clean surface of Mo foil. The CZTSSe film was deposited by spin-coating the precursor solution and then made selenized as done in our previous work.[21,22] The Cu (Aladdin, 99.9%, 1.10 mmol), Zn (Aladdin, 99.9%, 0.76 mmol), Sn (Alfa Aesar, 99.8%, 0.72 mmol), S (Aladdin, 99.9%, 2.7 mmol), and Se (Alfa Aesar, 99%, 0.3 mmol) powder were simultaneously dissolved in the liquid consisting of 1,2-ethanedithiol ($HSCH_2CH_2SH$, AR, 0.5 mL) and ethylenediamine ($H_2NCH_2CH_2NH_2$, AR, 5 mL), and the resulting solution needed magnetically stirring for 1.5 h at 70 °C. Then 1-mL stabilizer solution (ethanolamine ($HOCH_2CH_2NH_2$, AR): thioglycolic acid ($HSCH_2COOH$, 99%): 2-methoxyethanol ($HOCH_2CH_2OCH_3$, AR)=1:1:2) was injected into the solution, the resulting solution was stirred till it became golden yellow in color. Therefore, the precursor solution was obtained. In an argon-filled glovebox, the precursor films were prepared by spin-coating the precursor solution on Mo foils, followed by being baked on a hot plate (300 °C) for 1min. The procedure was repeated 9 times to obtain a film with a thickness of about 2.0 μm. Finally, the as-prepared precursor thin films were selenized at 550 °C for 15 min, and the CZTSSe films with good crystallinity were obtained. The CdS buffer layers were deposited by two methods (P-CBD and S-CBD) for contrastive analysis. The ZnO and ITO films were prepared by RF magnetron sputtering. The Ag collection grids with a thickness of 500 nm were subsequently deposited by thermal evaporation. Finally, a 0.21-cm^2 cell area was determined by a mechanical scribing step.

2.3. Characterizations and measurements

The surface morphologies were observed by a scanning electron microscope (SEM, Helios G4 CX). The surface roughness values were measured by an atomic force microscope (AFM, 5500). The transmittance spectra were measured with a UV-Vis spectrophotometer (Agilent CARY 5000 Scan). The photoluminescence spectra were measured by a Renishaw in Via Raman microscope using a 532-nm excitation wavelength. The current density–voltage (J–V) curves were measured with a Keithley 2400 source meter under the standard AM1.5 illumination (100 mW/cm^2). The external quantum efficiency (EQE) spectra were recorded using a CROWNTECH CT-SC-T QE system equipped with a 150-W xenon light source and a lock-in amplifier. The capacitance-voltage (C–V) curves were measured by using Keithley 4200 at a frequency of 50 kHz with a DC bias in a range from −1.0 V to 0 V. The compositions of CdS films were characterized by x-ray photoemission spectroscopy (XPS, ESCALAB 250). The electrochemical impedance spectroscopy (EIS) spectra were measured by using an electrochemical workstation (Bio-Logic SAS, VPS) at a DC bias voltage of 0 V with a frequency sweeping from 1 Hz to 1 GHz. Transient photovoltage (TPV) and transient photocurrent (TPC) were measured by an opto-electro-modulated transient photovoltage and photocurrent system.[23]

3. Results and discussion

High-quality CdS buffer layer plays an important role in performance of flexible CZTSSe solar cells. Hence, it is of great significance to study the deposition technique of the CdS film to improve PCE. In our previous work,[16,24] the CdS layer was deposited by the P-CBD method (see Fig. 1(a)), in which the $CdSO_4$ and thiourea powders were added into the reaction solution, successively. We observed some particles of thiourea could not dissolve immediately at the beginning of CdS deposition. Therefore, there appeared some problems with this approach. (i) When the $CdSO_4$ powder and thiourea powder were added into the reaction solution, part of them adhered to the surface of CZTSSe, which could destroy the smoothness and quality of the film and caused some holes in subsequent dissolution. (ii) The $CdSO_4$ powder and thiourea powder could not be dissolved quickly after they had been added into the reaction solution, so there were observed large particles in the solution, which is not conducive to the deposition of CdS thin film. (iii) The concentration of reaction solution gradually changed as the powder continued to dissolve, which could make the S content values in the obtained CdS film different so that the defects increased.

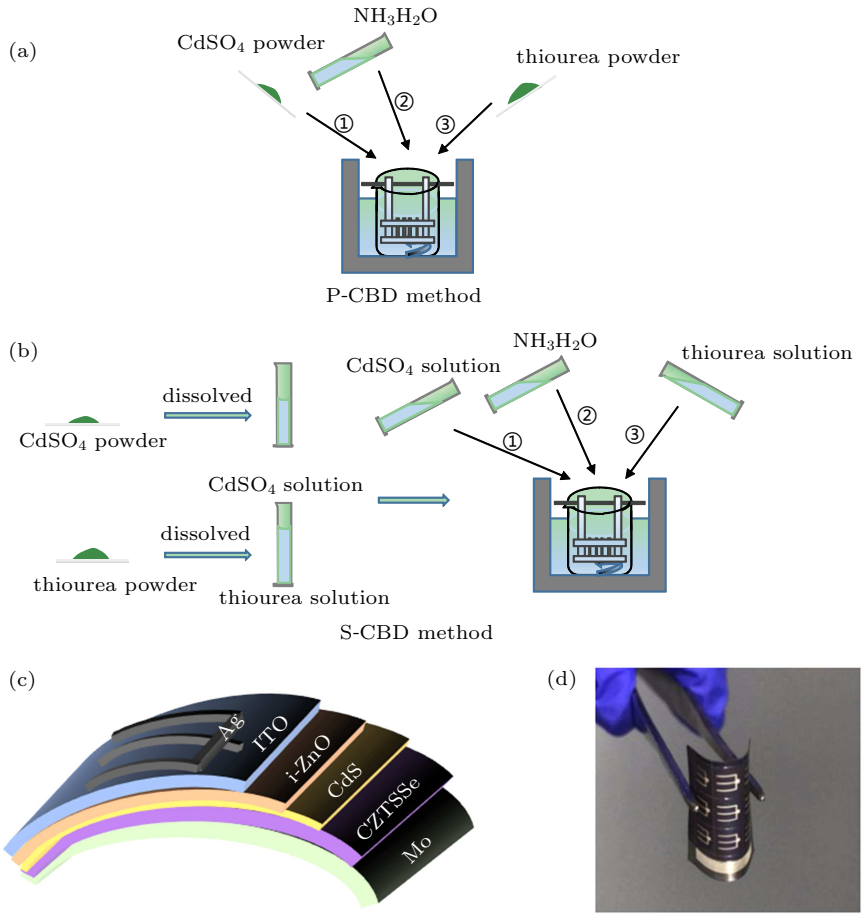


Fig. 1. Schematic diagram of (a) P-CBD method and (b) S-CBD method for depositing CdS films. (c) Schematic structure and (d) digital photograph of flexible Mo-foil-based CZTSSe solar cell.

Those might lead to poor CdS film quality, because the quality of CdS film heavily depended on precursor solution. To avoid these problems and improve CdS film quality, we first respectively prepare the thiourea solution and $CdSO_4$ solution. And then add them together to precursor solution to deposit the CdS film. The improved technique is named S-CBD as shown in Fig. 1(b). The S source and Cd source can be mixed uniformly for whole process. The CdS layers prepared by the two methods (P-CBD and S-CBD) are compared with each other and used to obtain high PCE of flexible CZTSSe solar cells. As shown in Fig. 1(c), the device structure is comprised of Mo foil/CZTSSe/CdS/i-ZnO/ITO/Ag. The Mo foil as a metal flexible substrate with superb flexibility and electrical conductivity shows large potential applications in CZTSSe solar cells.[12] When the device is irradiated, the electrons and holes can be successfully collected by Ag and Mo electrodes. The CdS layer is the most important part to deplete CZTSSe absorber and transport electrons.

The top-view SEM images of the CdS films prepared on the CZTSSe by the P-CBD method and S-CBD method are shown in Figs. 2(a) and 2(b), respectively. The SEM image of CZTSSe film is shown in Fig. S1 (supporting information). The CdS film prepared by the P-CBD method shows poor crystallization with lots of holes marked as red circles (Fig. 2(a)). Electrodes and absorber may contact each other in the hole region. And the pinholes would become trap centers resulting in V_{OC} loss in CZTSSe solar cells. The CdS film prepared by S-CBD method covers all the CZTSSe film, which is compact and has higher quality except several particles existent on the surface (Fig. 2(b)). From the transmittance spectra in Fig. 2(c), the CdS film prepared by the S-CBD method indicates higher transmittance from the smooth and compact surface of CdS film, thereby enhancing the light intensity reaching the CZTSSe layer underneath the CdS film.[25] The PL spectra of CdS films prepared by the two methods are shown in Fig. 2(d). The peak at 720 nm represents the defect emission, which reflects the CdS quality and defect state according to relevant literature.[26]. The defect emission of CdS film prepared by the S-CBD method sharply decreases, confirming fewer bulk defects and better crystalline quality.

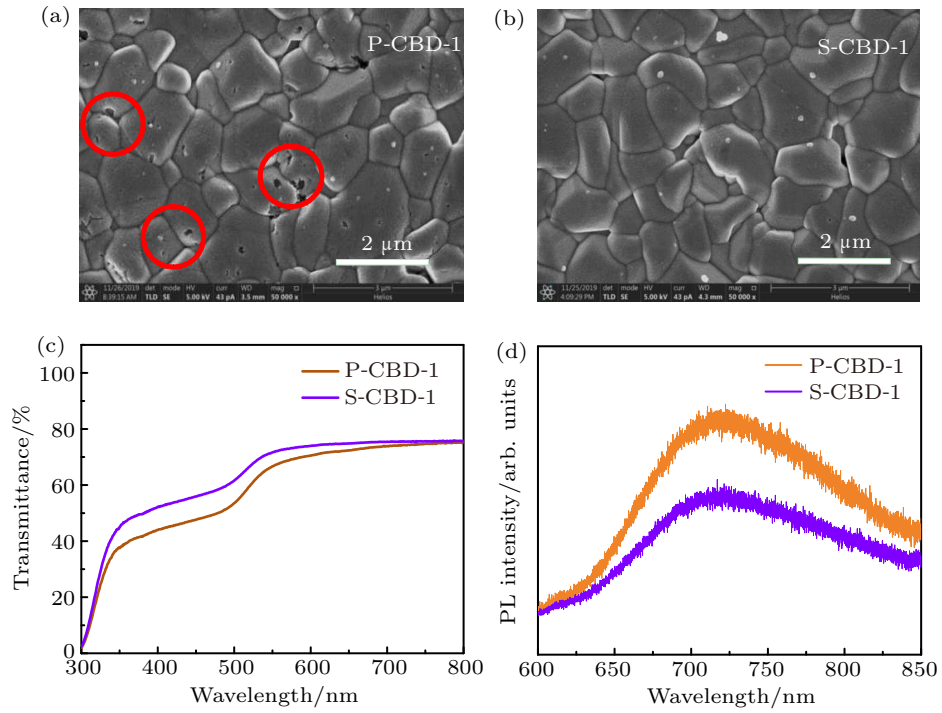


Fig. 2. Top-view SEM images of the CdS films prepared on CZTSSe films by (a) P-CBD method and (b) S-CBD method. (c) UV–Vis transmittance spectra and (d) PL spectra of CdS films.

The performances of flexible CdS/CZTSSe solar cells prepared by the P-CBD method and S-CBD method are further contrastively investigated. We measure the device performances in statistics of 20 samples. As shown in Fig. 3(a), the PCE s of flexible CdS/CZTSSe solar cells of S-CBD-1 are spread over a range of 5.77%–6.86%, much higher than those of P-CBD-1 devices (4.79%–5.70%). The statistical distribution of performance indicates that S-CBD-1 devices possess good reproducibility and effectiveness of performance improvement. Comparing with the influence on J_{SC} and FF (Fig. S2), the V_{OC} (Fig. 3(b)) reveals significant improvement by 7.5%. As shown in Fig. S2(a), the S-CBD-1 device shows better junction interface according to less V_{OC} deficit ($V_{OC,def} = E_g/q - V_{OC}$) of 0.701 V. The J–V curves of the champion P-CBD-1 device and S-CBD-1 device are shown in Fig. 3(c). The champion solar cell of S-CBD-1 obtains a PCE of 6.86% with a V_{OC} of 0.374 V, a J_{SC} of 31.37 mA/cm^2, and an FF of 58.54%, which demonstrate the superior per-

formance than that of P-CBD-1 device especially in V_{OC} and *FF*. The EQE spectra of P-CBD-1 device and S-CBD-1 device are described in Fig. 3(d). The EQEs of S-CBD-1 devices are significantly enhanced in a range of 520 nm–800 nm. And the EQE values are over 85% at the wavelengths in a range of 540 nm–690 nm. The increase of the EQE at shorter wavelengths for champion device is attributed to the decrease in parasitic absorption due to better quality of CdS film.[27] The integrated current densities are 30.27 mA/cm^2 and 30.93 mA/cm^2 for the P-CBD-1 device and S-CBD-1 device, according with the *J*–*V* curves, respectively.

The CZTSSe/CdS heterojunction interface properties from the P-CBD method and S-CBD method are further analyzed by physical measurements. The PN junction ideal factor (A) plays an important role in separating the electron–hole pairs at the junction interface. These parameters can be derived from the abrupt junction *J*–*V* equation[28]

$$J = J_0\left[\exp\frac{q}{AkT}(V - JR_s) - 1\right] + G_{sh}(V - JR_s) - J_L, \quad (1)$$

where J_L is the photogeneration current density, J_0 is the reverse saturation current density, q is the electron charge, R_s is the series resistance, and G_{sh} is the shunt conductance.

The derivative of Eq. (1) with respect to J is as follows:

$$\frac{dV}{dJ} = R_s + \frac{AkT}{q}(J + J_{SC})^{-1}. \quad (2)$$

The plots of dJ/dV against V are shown in Fig. 4(a). The G_{sh} value is extracted from a flat region under reverse bias.[29] The G_{sh} value of P-CBD-1 device and S-CBD-1 device are 9.56 mS/cm^2 and 5.03 mS/cm^2, respectively. Figure 4(b) shows the plots of dV/dJ over $(J + J_{SC})^{-1}$ from Eq. (2). The R_s and A are derived from an intercept (R_s) and a slope (AkT/q) of a linear fit to the curve, respectively. The series resistance and PN junction quality factor of P-CBD-1 based device and S-CBD-1 based device are $R_s = 0.67\ \Omega{\cdot}cm^2$, $A = 2.62$, and $R_s = 0.73\ \Omega{\cdot}cm^2$, $A = 2.09$, respectively. For P-CBD-1 device and S-CBD-1 device, their J_0 values are extracted to be 0.09 mA/cm^2 and 0.015 mA/cm^2 from the plots of $J + J_{SC} - G_{sh}V$ *versus* V–JR_s (Fig. 4(c)), respectively. As seen from the above, the S-CBD-1 device has a better ideal factor A, smaller G_{sh} and J_0. The improvement from 2.62 to 2.09 of A indicates that the carrier recombination is inhibited at the junction interface.[30,31] The decrease in J_0 and G_{sh} suggests that the junction quality is promoted, improving the overall performance of the device.

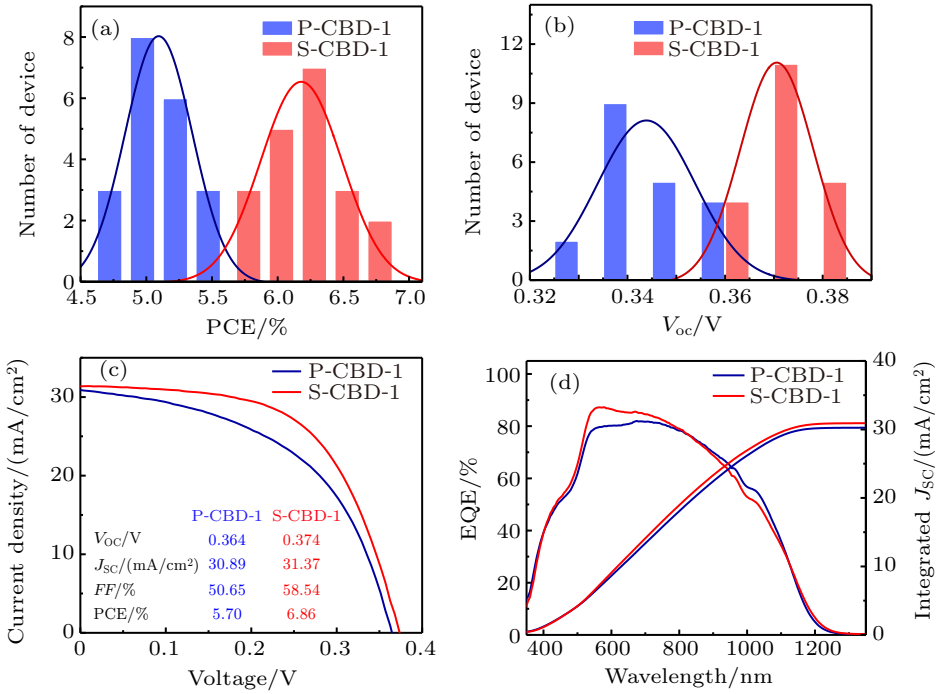


Fig. 3. Plots of statistical distribution of (a) PCE and (b) V_{OC} from 20 devices for each group. (c) *J*–*V* curves and (d) EQE spectra of P-CBD-1 device and S-CBD-1 device.

The built-in voltage (V_{bi}), depletion width (W_d) and carrier density (N_{C-V}) are deduced from capacitance–voltage (*C*–*V*) curves to further analyze PN junction information. The dielectric constant of the CZTSSe layer at different frequencies (Fig. S3(b)) is determined by measuring the capacitance-frequency of the parallel plate capacitor mode (Fig. S3(a)). The dielectric constant at 50 kHz is 16.21 for parameter calculation. As shown in Fig. 4(d), the V_{bi} is extracted from the extrapolated horizontal axis intercept of linear fitting of the $C^{-2} \sim V$ curve. The V_{bi} of S-CBD-1 device (0.67 V) is 100 mV higher than that of P-CBD-1 device (0.57), which contributes to higher V_{OC}.[32] The carrier density and depletion

width calculated from the *C*–*V* curves are shown in Fig. 4(e). The carrier density N_{C-V} of P-CBD-1 device and S-CBD-1 device are the same value, on order of 10^{15} cm^{-3}, indicating that the CZTSSe films have no obvious change after follow-up CBD process. As shown in Fig. 4(f), the W_d of CBD-1 device (539 nm) is 40 nm wider than that of P-CBD-1 device (499 nm). The enhancement of W_d originates from higher carrier concentration and better crystallization of the CdS layer prepared by the S-CBD method. The wider W_d and larger V_{bi} could reduce the interface recombination and conduce to more efficiently collecting carriers and ensuring high efficiency of CZTSSe solar cells.

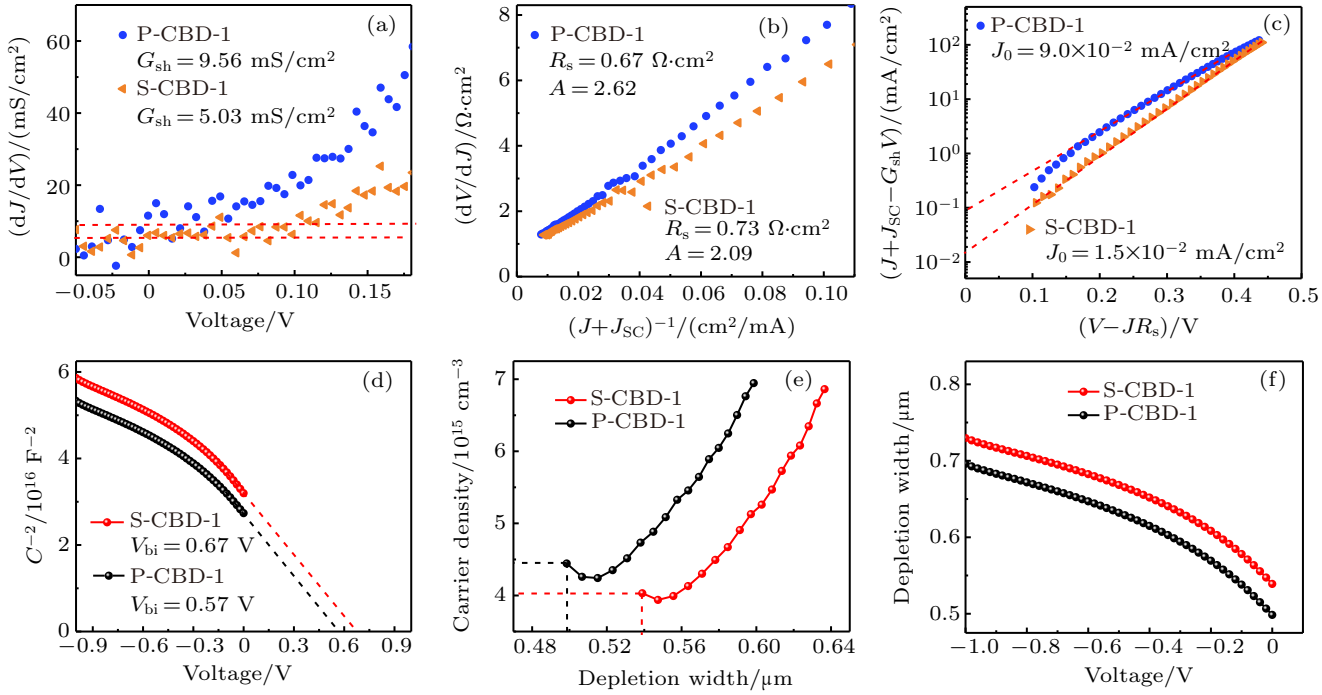


Fig. 4. Plots of (a) dJ/dV against voltage, (b) dV/dJ *versus* $(J+J_{SC})^{-1}$, (c) $J+J_{SC}-G_{sh}V$ *versus* V–JR_s, (d) C^{-2}–V, (e) carrier density *versus* depletion width, and (f) depletion width *versus* voltage for P-CBD-1 and S-CBD-1 devices.

The performances of S-CBD-1 device have been greatly improved, but there are still observed several particles in the CdS layer deposited by the S-CBD method (Fig. 2(b)). We then analyze the composition of the CdS film based on the S-CBD method by XPS. The XPS spectra of Cd 3d and S 2p in the CdS film are described in Fig. S4(a) and S4(b). There are no changes in the valence state of Cd and S, which are well consistent with previous reports.[33,34] According to XPS survey data, the atomic ratio of Cd and S in the CdS film is 1:0.89, indicating that S element is insufficient in the CdS film. Probably some of the S atoms are easily lost during the CdS deposition, which can cause defects and affect device performance. There is a chemical engineering-type model of the CdS deposition process:[35]

$$NH_3\cdot H_2O \rightleftharpoons NH_4^+ + OH^-, \tag{3}$$

$$SC(NH_2)_2 + OH^- \rightarrow HS^- + CN_2H_2 + H_2O, \tag{4}$$

$$HS^- + OH^- \rightleftharpoons S^{2-} + H_2O, \tag{5}$$

$$Cd^{2+} + S^{2-} \rightleftharpoons CdS\,(s). \tag{6}$$

The model equations (3)–(6) show that thiourea is the S source of CdS. According to reversible equations (5) and (6), the increase of thiourea will promote the generation of more CdS and reduce the absence of S atoms. To prove the above, we increase the thiourea concentration to 0.68 mol/L. The XPS spectra of Cd 3d and S 2p in the CdS film are shown in Figs. S4(c)–S4(d). The atomic ratio of Cd to S in the CdS film is 1:0.999 extracted from XPS survey data, indicating that the loss of S in CdS film can be reduced by increasing the amount of thiourea during deposition. Therefore, we control the content of S in the CdS deposition process to further improve the device performance.

In order to reduce the defects due to S loss, we increase the thiourea solution concentration (S source) to 0.34 mol/L (5 times 0.068 mol/L), 0.68 mol/L (10 times 0.068 mol/L), and 1.02 mol/L (15 times 0.068 mol/L) separately. The CdS film samples are named S-CBD-5, S-CBD-10, S-CBD-15, respectively. And the top-view SEM images of different CdS layers are shown in Figs. 5(a)–5(c). The CdS layer deposited by increasing the content of S source shows higher density and better crystallization without particles than the general CdS layer (Fig. 2(b)), which might result in larger *FF* of device.[36] The different S-CBD CdS films prepared on the soda lime glasses are characterized by atomic force microscopy (AFM) to further investigate the influence of S source on CdS film quality. As shown in Figs. 5(d)–5(f), when the S source concentration increases from 0.34 mol/L to 0.68 mol/L, the CdS film be-

comes much denser with particle diameter increasing. When the S source concentration increases to 1.02 mol/L, the CdS particle diameter increases and the membrane becomes loose. The average roughness (R_a) values of the different CdS films are 8.47, 7.75 and 20.8 nm, respectively. Hence, the CdS film has a minimum roughness when the concentration of S source is 0.68 mol/L, which can lead the CdS film to better contact the CZTSSe film[37] and improve the CZTSSe/CdS interface quality.

The statistical distributions of PCE, V_{OC}, J_{SC}, FF from 20 devices for each group are shown in Figs. 6(a)–6(d). Compared with those of the S-CBD-1 devices, the PCE and V_{OC} of increased S source devices are significantly improved, which is attributed to the improved quality of CdS film and CZTSSe/CdS interface. And the performances of S-CBD-10 devices are achieved optimally. However, the performances of S-CBD-15 devices decrease rapidly. The excess S source makes the CdS particles too large so that the CdS film is loose and rough, which affects the CZTSSe/CdS interface quality and ultimately leads the performance of the device to degrade.

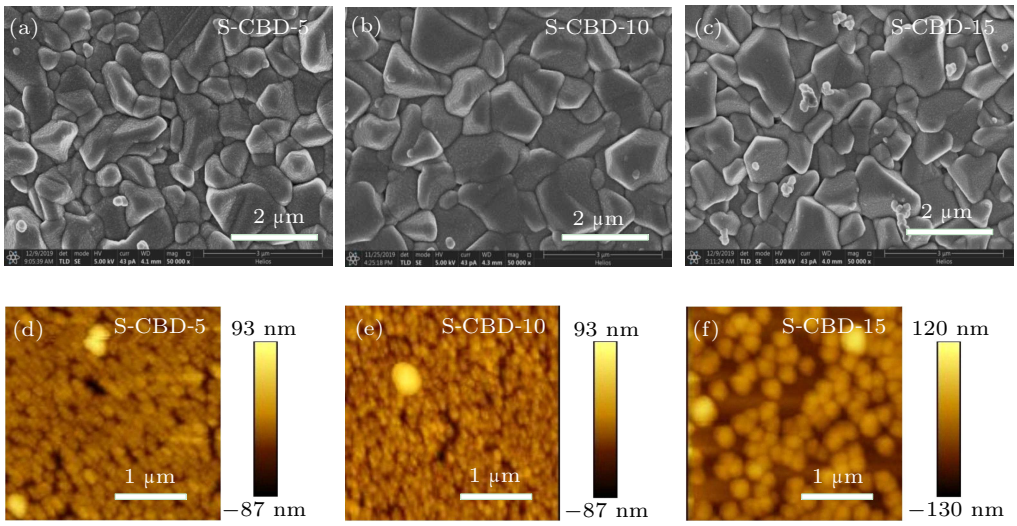


Fig. 5. Top-view SEM images of CdS films on CZTSSe prepared by S-CBD method with S source concentration of (a) 0.34 mol/L, (b) 0.68 mol/L, and (c) 1.02 mol/L. AFM images of S-CBD CdS films on glass with S source concentration of (d) 0.34 mol/L, (e) 0.68 mol/L, and (f) 1.02 mol/L.

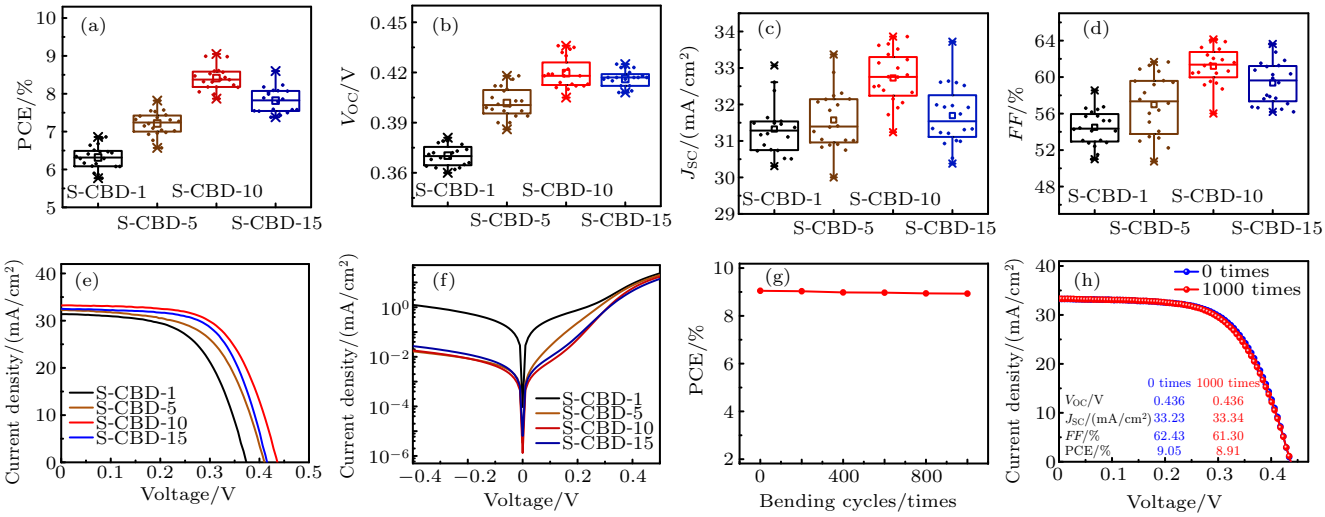


Fig. 6. Plots of statistical distribution of (a) PCE, (b) V_{OC}, (c) J_{SC}, and (d) FF from 20 devices for each group. (e) J–V curves, (f) dark J–V curves, (g) PCE *versus* bending cycle, and (h) J–V curves of device that is bent 0 and 1000 times.

The light and dark J–V curves for the solar cells with different content of S source are described in Figs. 6(e) and 6(f), respectively. The key parameters of the compared devices are listed in Table 1. By increasing the content of S source for CdS film, the device performances are significantly better than those of the S-CBD-1 device especially V_{OC}. The S-CBD-10 device achieves optimal parameters and the champion device obtains the PCE of 9.05% with the V_{OC} of 0.436 V, J_{SC} of 33.23 mA/cm^2 and FF of 62.43%. Compared with the value of V_{OC} for S-CBD-1 device (0.374 V), the V_{OC} of S-CBD-10 device shows a significant enhancement of 16.6%. As shown in Table 1, the S-CBD-10 device achieves optimal diode properties because of best ideality factor, the smallest G_{sh} and the lowest J_0. However, R_s of the S-CBD-15 device is greater

than those of other group devices, demonstrating that the excess S source increases R_s and reduces the ability to transfer charges, thereby degrading the device performance. In consequence, the junction quality is significantly promoted by increasing the content of S source. Mechanical flexibility and durability are the important indexes of practicality for flexible device.[16] The device is bent outwards 200, 400, 600, 800, and 1000 times from a radius of 6 mm and then the sample is taken back into planar state for testing (Figs. 6(g)–6(h)). After being bent 1000 times bends, the device retains 98.5% of its original efficiency, showing that the CZTSSe devices have excellent mechanical flexibility and durability.

Table 1. Related parameters of CZTSSe solar cells with CdS film deposited in different S-source concentrations.

Sample	PCE/%	V_{OC}/V	J_{SC}/(mA/cm^2)	FF/%	J_0/(mA/cm^2)	A	G_{sh}/(mS/cm^2)	R_s/Ω·cm^2
S-CBD-1	6.86	0.374	31.37	58.54	1.5×10^{-2}	2.09	5.03	0.73
S-CBD-5	7.82	0.410	32.24	59.18	5.5×10^{-3}	1.83	4.22	0.96
S-CBD-10	9.05	0.436	33.23	62.43	9.0×10^{-4}	1.64	2.25	0.96
S-CBD-15	8.60	0.416	32.52	63.63	3.0×10^{-3}	1.80	3.06	1.62

The physical origins of improving the device performance are explored by analyzing the C–V data (Fig. S5). The values of carrier density N_{C-V} of all groups of devices are the same, on the order of 10^{15} cm^{-3}. The maximum value of V_{bi} and W_d are obtained when the CdS layer is deposited by the S-CBD method with a 0.68 mol/L S source. The V_{bi} with increased S source device is 0.85 V, 0.18 V higher than that of S-CBD-1 device (0.67 V). The S source control can effectively improve the CZTSSe/CdS interface and suppress the interfacial recombination, which is the reason why the value of V_{OC} can be improved.

The interface information of the device can be clearly analyzed by electrochemical impedance spectroscopy (EIS).[38] The junction interface can be described as a circuit consisting of an ideal capacitor and a resistance, which are connected in parallel . The Nyquist diagrams of EIS spectra are described in Fig. 7(a). The series resistance (R_s) and recombination resistance (R_{rec}) can be obtained from the x-axis intersections of the circular curve at high and low frequency, respectively. The diameter of the circle line of the impedance spectrum represents the size of the shunt resistance (R_{sh}). With the increase of S source for CdS film, the R_{rec} value increases from 4.2 kΩ to 10 kΩ and then decreases to 8 kΩ under zero bias voltage. As shown in Fig. 7(b), the R_{rec} value of each group decreases with the increase of bias voltage and its variation law under the same bias voltage is consistent with the variation law of R_{rec} under zero bias voltage. Therefore, increasing S source (0.68 mol/L) in the deposition process can reduce the vacancy of the CdS layer and suppress the defect recombination at the interface.[20] However, the R_{rec} of device decreases because excess S source introduces new recombination centers into the CZTSSe/CdS interface.

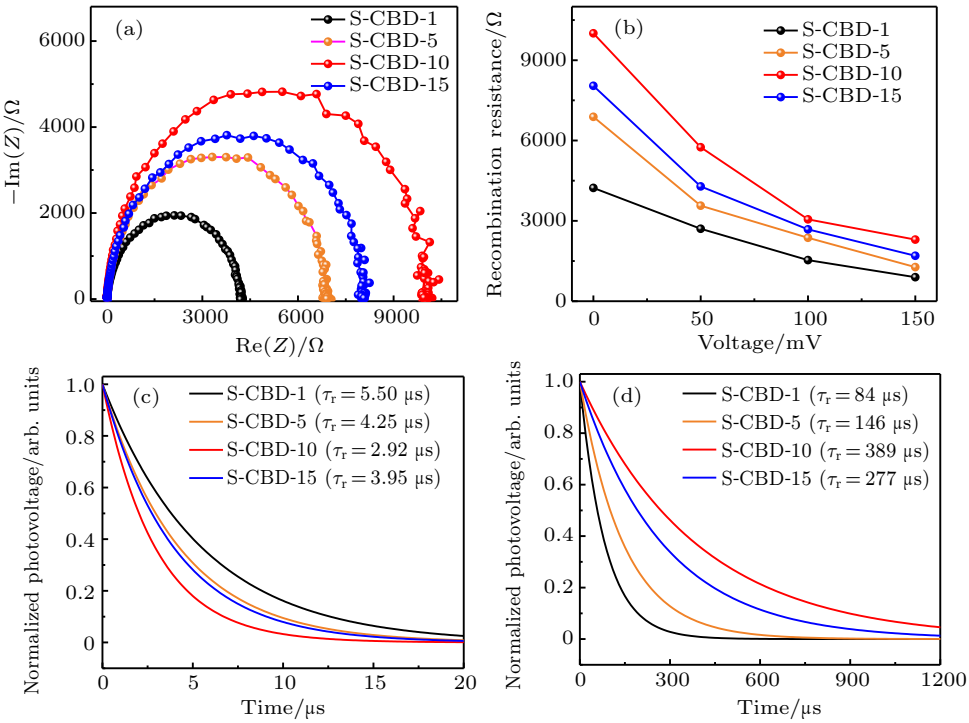


Fig. 7. (a) Impedance spectra and (b) bias voltage-dependent recombination resistance curves for devices based on CdS film deposited in different S source concentrations. (c) TPC decay and (d) TPV decay of typical devices.

The different CdS layer based devices are further investigated through transient photocurrent (TPC) and transient photovoltage (TPV) measurements to analyze charge transfer and recombination in CZTSSe solar cell.[39] The charge transfer lifetime (τ_t) can be calculated from the TPC decay of device under the condition of short circuit and characterize the ability of device to extract and transfer charge.[40] As shown in Fig. 7(c), the values of τ_t for the devices under the increasing S source condition are calculated to be 5.50, 4.25, 2.92, and 3.95 μs, respectively. The device based on CdS film with increased S source indicates better charge extraction and transport effect. The charge recombination lifetime (τ_r) can be derived from the TPV decay of device to characterize charge recombination and trap density in device.[41,42] With the increase of S source for CdS film, the τ_r of the device becomes much longer than that of the S-CBD-1 device (Fig. 7(d)), demonstrating the charge recombination density decreases after S has been supplemented. Hence, the recombination in CZTSSe/CdS heterojunction interface is obviously suppressed for the high efficiency solar cells by increasing appropriate S source (0.68 mol/L) during the CdS deposition.

4. Conclusions and perspectives

In this work, the deposition process of CdS buffer layers and junction interface properties are investigated to obtain high-efficiency flexible Mo-foil-based CZTSSe solar cells. Comparing with the P-CBD method, the CdS layer deposited by the S-CBD method shows high crystalline quality without any pinholes. The PCE of the device is enhanced to 6.86%. The *J*–*V* and *C*–*V* characteristics of the devices demonstrate that the buffer layers deposited by the S-CBD method can improve carrier collection efficiency and reduce V_{OC} deficit. To reduce S loss in CdS film, we control the S source during the CdS deposition. When S source is increased to 0.68 mol/L, the PCE of the champion flexible CZTSSe solar cells on Mo foil reaches 9.05%, which is much higher than that (6.86%) of original device. The improvement mechanism is revealed through systematical physical characterizations. With the increase of S source, the V_{bi} and W_d of PN junction are obviously enhanced, and the recombination resistance increases from 4.2 kΩ to 10 kΩ. The charge transfer lifetime and the charge recombination lifetime arrive at 2.92 μs and 389 μs, respectively. The quality of CZTSSe/CdS heterojunction interface in CZTSSe solar cells is notably improved due to S supplement and defect passivation. Moreover, the device efficiency decreases only by 1.5% after being bent 1000 times, showing excellent flexibility characteristics. That makes CZTSSe solar cells flexible for a variety of applications. The present strategy of the CdS buffer layer deposition and heterojunction interface are expected to greatly enrich the research of the kesterite thin film solar cells and further improve their performances.

Acknowledgment

The authors thank the Testing center of Fuzhou University for the testing facility.

References

[1] Chen Y S, Wang Y J, Li R, Gu J H, Lu J X and Yang S E 2012 *Chin. Phys. B* **21** 058801
[2] Jiang Z W, Gao S S, Wang S Y, Wang D X, Gao P, Sun Q, Zhou Z Q, Liu W, Sun Y and Zhang Y 2019 *Chin. Phys. B* **28** 048801
[3] Li Y M, Qiu L X, Ding Z H, Li Y F, Yao B, Xiao Z Y and Zhu P W 2016 *Chin. Phys. Lett.* **33** 076101
[4] Sun D, Ge Y, Xu S Z, Zhang L, Li B Z, Wang G C, Wei C C, Zhao Y and Zhang X D 2015 *Chin. Phys. Lett.* **32** 128401
[5] Yu J, Zheng Z, Dong L, Cheng S, Lai Y, Zheng Q, Zhou H, Jia H and Zhang H 2017 *Chin. Phys. B* **26** 046802
[6] Li J, Wang D, Li X, Zeng Y and Zhang Y 2018 *Adv. Sci.* **5** 1700744
[7] Yang K J, Kim S, Kim S Y, Ahn K, Son D H, Kim S H, Lee S J, Kim Y I, Park S N, Sung S J, Kim D H, Enkhbat T, Kim J, Jeon C W and Kang J K 2019 *Nat. Commun.* **10** 2959
[8] Wang W, Shen H L, Jin J L, Li J Z and Ma Y 2015 *Chin. Phys. B* **24** 056805
[9] Polman A, Knight M, Garnett E C, Ehrler B and Sinke W C 2016 *Science* **352** aad4424
[10] Zhang J, Liao J, Shao L X, Xue S W and Wang Z G 2018 *Chin. Phys. Lett.* **35** 083101
[11] Sun K, Yan C, Huang J, Liu F, Li J, Sun H, Zhang Y, Cui X, Wang A, Fang Z, Cong J, Lai Y, Green M A and Hao X 2019 *J. Mater. Chem. A* **7** 27289
[12] Lin S H and Cheng T H 2016 *Jpn. J. Appl. Phys.* **55** 06GL06
[13] Wei Y, Zhuang D, Zhao M, Zhang W, Ren G, Wu Y, Sun R, Gong Q, Zhang L, Zhan S, Peng X and Lyu X 2018 *Solar Energy Materials and Solar Cells* **180** 19
[14] Zhang S, Yu F, Yuan Q, Wang Y, Wei S, Tesfamichael T, Liang B and Wang H 2019 *Solar Energy Materials and Solar Cells* **200** 109892
[15] Sun H, Sun K, Huang J, Yan C, Liu F, Park J, Pu A, Stride J A, Green M A and Hao X 2017 *ACS Appl. Energy Mater.* **1** 154
[16] Yan Q, Cheng S, Li H, Yu X, Fu J, Tian Q, Jia H and Wu S 2019 *Solar Energy* **177** 508
[17] Liu F, Lai Y, Liu J, Wang B, Kuang S, Zhang Z, Li J and Liu Y 2010 *J. Alloys Compd.* **493** 305
[18] Mann J R, Vora N and Repins I L 2010 *Solar Energy Materials and Solar Cells* **94** 333
[19] Weber M, Krauser J, Weidinger A, Bruns J, Fischer C H and Bohne W 1999 *J. Electrochem. Soc.* **146** 2131
[20] Khan J, Yang X, Qiao K, Deng H, Zhang J, Liu Z, Ahmad W, Zhang J, Li D, Liu H, Song H, Cheng C and Tang J 2017 *J. Mater. Chem. A* **5** 17240
[21] Yu X, Cheng S, Yan Q, Fu J, Jia H, Sun Q, Yang Z and Wu S 2020 *Solar Energy Materials and Solar Cells* **209** 110434
[22] Yan Q, Cheng S, Yu X, Jia H, Fu J, Zhang C, Zheng Q and Wu S 2019 *Solar RRL* **4** 1900410
[23] Shi J, Li D, Luo Y, Wu H and Meng Q 2016 *Rev. Sci. Instrum.* **87** 123107
[24] Yu X, Cheng S, Yan Q, Yu J, Qiu W, Zhou Z, Zheng Q and Wu S 2018 *RSC Adv.* **8** 27686
[25] Ke W, Zhao D, Cimaroli A J, Grice C R, Qin P, Liu Q, Xiong L, Yan Y and Fang G 2015 *J. Mater. Chem. A* **3** 24163
[26] Zhang G, Jiang S, Lin Y, Ren W, Cai H, Wu Y, Zhang Q, Pan N, Luo Y and Wang X 2014 *J. Mater. Chem. A* **2** 5675
[27] Ishaq M, Deng H, Yuan S, Zhang H, Khan J, Farooq U, Song H and Tang J 2018 *Solar RRL* **2** 1800144
[28] Li Q, Shen K, Yang R, Zhao Y, Lu S, Wang R, Dong J and Wang D 2017 *Solar Energy* **157** 216

[29] Wang H, Wang Y, He B, Li W, Sulaman M, Xu J, Yang S, Tang Y and Zou B 2016 *ACS Appl. Mater. Interf.* **8** 18526
[30] Wang W, Winkler M T, Gunawan O, Gokmen T, Todorov T K, Zhu Y and Mitzi D B 2014 *Adv. Energy Mater.* **4** 1301465
[31] Deng H, Zeng Y, Ishaq M, Yuan S, Zhang H, Yang X, Hou M, Farooq U, Huang J, Sun K, Webster R, Wu H, Chen Z, Yi F, Song H, Hao X and Tang J 2019 *Adv. Funct. Mater.* **29** 1901720
[32] Hu X, Tao J, Chen S, Xue J, Weng G, Kaijiang, Hu Z, Jiang J, Chen S, Zhu Z and Chu J 2018 *Solar Energy Materials and Solar Cells* **187** 170
[33] Gaarenstroom S W and Winograd N 1977 *J. Chem. Phys.* **67** 3500
[34] Wang L, Luo M, Qin S, Liu X, Chen J, Yang B, Leng M, Xue D J, Zhou Y, Gao L, Song H and Tang J 2015 *Appl. Phys. Lett.* **107** 143902
[35] Kostoglou M, Andritsos N and Karabelas A J 2000 *Industrial & Engineering Chemistry Research* **39** 3272
[36] Yang G, Tao H, Qin P, Ke W and Fang G 2016 *J. Mater. Chem. A* **4** 3970
[37] Zhang A, Zhou Z, Zhou W, Kou D, Meng Y, Qi Y, Yuan S and Wu S 2019 *Solar RRL* **3** 1900131
[38] Leever B J, Bailey C A, Marks T J, Hersam M C and Durstock M F 2012 *Adv. Energy Mater.* **2** 120
[39] Pang S, Zhang C, Dong H, Chen D, Zhu W, Xi H, Chang J, Lin Z, Zhang J and Hao Y 2019 *ACS Appl. Energy Mater.* **2** 4700
[40] Yan W, Huo M M, Hu R and Wang Y 2019 *RSC Adv.* **9** 1734
[41] Jiang Q, Zhang L, Wang H, Yang X, Meng J, Liu H, Yin Z, Wu J, Zhang X and You J 2016 *Nat. Energy* **2** 1
[42] Min X, Shi J, Guo L, Yu Q, Zhang P, Tian Q, Li D, Luo Y, Wu H, Meng Q and Wu S 2018 *Chin. Phys. B* **27** 016402